






Cite this: DOI: 10.1039/d5py00872g

Diversity-oriented route to functional covalent triazine frameworks

Catherine Mollart,  * Ellena Sherrett, Patrick Heasman, Michael J. G. Peach, 
Adam Rowling, Lewis J. Beck, Ellie Varley, David Seed and Abbie Trewin  *

An alternative route to synthesise TCNQ-CTF by using trifluoromethanesulfonic (TFMS) acid catalysis is presented, in comparison to a previously reported ZnCl_2 -catalysed synthesis. The new synthetic route yields a polymer with additional structural diversity compared to the previously reported material. The composition of the framework is rationalised by 'artificial' acid-catalysed synthesis of TCNQ-CTF, together with a novel approach to structural feature identification, with a range of alternative structural features appearing that were not present in the previously reported polymer formed by ZnCl_2 catalysis. These results will inform the design of new CTF materials with additional functionality and broader applications.

Received 5th September 2025,
Accepted 19th November 2025

DOI: 10.1039/d5py00872g

rsc.li/polymers

Introduction

There is increasing demand for functional materials that can power electronic devices and capture greenhouse gases, among a large range of other applications. There have been recent reports of functional polymer materials that pave the way towards this long-term goal, and discovery and design of such materials is a rapidly growing field.^{1–10}

One class of such functional polymer materials are covalent triazine frameworks (CTFs), with applications in areas such as carbon dioxide capture,^{11,12} drug delivery,¹³ heterogeneous catalysis,¹⁴ and photocatalysis.^{11,15} These are microporous polymer materials with a covalent, π -conjugated skeleton, first reported in 2008 by Kuhn and co-workers.¹⁶ The original CTF material, CTF-1, was formed using a high-temperature ionothermal synthesis of 1,4-dicyanobenzene, catalysed using one equivalent of molten ZnCl_2 .¹⁶ The resulting material was highly porous (with a Brunauer–Emmett–Teller [BET] surface area of $791 \text{ m}^2 \text{ g}^{-1}$), chemically and thermally stable, and crystalline, with an analogous stacked topology to covalent organic framework (COF)-1.¹⁶

Whilst molten ZnCl_2 is a suitable catalyst for CTF formation, it proves challenging to separate the catalyst from the product.¹¹ This led Ren and co-workers to investigate more facile synthetic routes to CTF synthesis; operating at room temperature or under microwave-assisted conditions in the presence of trifluoromethanesulfonic (TFMS) acid catalyst, with a much-reduced reaction time and no reduction in chemical stability.¹¹

However, unlike the original ZnCl_2 -catalysed CTF materials, which were synthesised under thermodynamic control, the acid catalysed CTFs are kinetic products, exhibiting little to no order within the structures. Additionally, the TFMS-catalysed CTFs synthesised at room temperature and under microwave-assisted conditions using the same monomer as CTF-1 (named P1 and P1M, respectively) display reduced porosity in comparison to the crystalline CTF-1 material, demonstrating the synthetic route employed in CTF preparation is a key influence on the structure and properties of the polymer.¹⁷ A comparison of the synthetic routes utilised to make CTF-1, P1M and P1, and the properties of the resulting materials, are given in Scheme S1 and Table S1.

CTF materials synthesised from tetracyanoquinodimethane (TCNQ) by Li and co-workers (Scheme S2), named TCNQ-CTFs, showed intriguing properties as electrodes for supercapacitor materials due to their high surface areas and nitrogen content (with observed values of greater than $3600 \text{ m}^2 \text{ g}^{-1}$ and 8%, respectively).¹⁸ Yet despite being synthesised using a high temperature molten ZnCl_2 -catalysed reaction, which has previously been the default synthetic route to crystalline CTFs, the resulting TCNQ-CTFs were amorphous as judged by powder X-ray diffraction (PXRD, Fig. S2).¹⁸

We have ourselves previously rationalised the FT-IR spectrum of the amorphous P1 material by generating snapshots of its structure using our in-house code Ambuild, which is designed to model amorphous microporous polymers under kinetic control.¹⁷ By generating P1 structures using Ambuild, a range of structural diversity beyond the expected triazine ring thermodynamic product was observed, arising from the kinetic control of the reaction. IR spectra were calculated for fragments observed in the generated structure; it was found the peaks, in combination with adsorbed CO_2 , H_2O and H_3O^+

Department of Chemistry, Lancaster University, Lancaster, LA1 4YB, UK.
E-mail: a.trewin@lancaster.ac.uk, c.l.mollart@bham.ac.uk



guests, matched the additional peaks in the P1 FT-IR spectrum compared to the spectrum of the crystalline CTF-1 product.

In this work, we have synthesised TCNQ-CTF using the TFMS-catalysed reaction (Fig. 1). We rationalise the structure of TCNQ-CTFs using 100 models of TCNQ-CTF clusters, each grown independently to contain 10 TCNQ building blocks. By generating this series of small clusters, we can assess the range of structural diversity present and the prevalence of each observed structural feature across our dataset. This approach is a variation on a protocol we recently established in ref. 19 for the study of amorphous pyrene-based conjugated microporous polymers.¹⁹ Further we establish an automated protocol for the substructure counting process by searching for the SMILES (simplified molecular line entry system) strings of each of the identified structural features within the clusters using RDKit in Python. This allows our models to be rapidly analysed in a more high-throughput manner using a method readily adaptable to the study of new materials. Using fragments representing the identified structural features, we calculated the infrared (IR), nuclear magnetic resonance (NMR) and UV-Vis spectra of each structural feature observed within the models, to produce an overall spectrum representative of the experimental material. The increased functionality of our materials in comparison with the original synthesis route results in a structure that more closely resembles covalent adaptable networks (CANs)^{20–22} and thus increases their range of functionalities. These include but are not limited to shape tune-

ability, recyclability and self-healing properties due to their smart response to thermal or photochemical stimuli.²³ This is particularly important in the current global strive towards reduction, reuse and recycling of waste materials, in line with the United Nations Sustainable Development Goals.²⁴

Methodology

TCNQ-CTF was synthesised at room temperature using TFMS acid-catalysed cyclotrimerisation. More details and the reaction scheme can be found in Scheme S3. FT-IR spectra were collected on an Agilent Cary 630 FT-IR spectrometer from 4000–650 cm^{-1} at 2 cm^{-1} resolution (Fig. S5). UV-Vis absorption spectra were collected on an Avantes AvaSpec-2048FT spectrometer with a Thorlabs SLS201/M stabilized fibre-coupled light source (Fig. S6). Solid state NMR spectra were collected using a Bruker AVANCE III HD 400 WB spectrometer (Fig. S8). Scanning electron microscopy was performed using a Jeol JSM-5600 SEM (Fig. S9). Powder X-ray diffraction was performed using a Rigaku SmartLab Multipurpose X-Ray Diffractometer, where solid powder samples were ground and loaded onto quartz plates (Fig. S3).

Previously, we have successfully used Ambuild to generate P1 network models.¹⁷ Here we can apply the same strategy with details of the mechanism given in Fig. S1. Full details of the Ambuild network generation procedure can be found in section S2, however a brief description of the process is as follows. Firstly, one TCNQ building block is seeded into a cell and a *growBlocks* step used to bond a second block to the first, thus mimicking the next step in the mechanism. A free end group is randomly identified by the Ambuild code, and a further building block is attached, following bonding rules that a carbon end group can only bond to a nitrogen end group and *vice versa*. The orientation of the attached building block is determined by the cap atom vectors and any close contacts with other atoms in the cell. The hydrogen cap atoms are removed once a successful bond is formed, leading to intermediate 2. This process is repeated to produce intermediate 3. A *zipBlocks* test is undertaken to form a triazine ring from intermediate 3, where each end group is tested for the possibility of forming a bond between it and neighbouring end groups by measuring the distance and angle between them against pre-determined criteria. If the *zipBlocks* test is successful, the two cap atoms are removed and a bond is formed between the end groups. This is repeated until 10 building blocks have been grown onto the network, and any further bonding has been tested, shown in Fig. 2.

We have previously determined the parameters used within Ambuild to describe the bonds, angles and dihedrals using a simplified test mechanism, calibrating against structures obtained from the polymer consistent forcefield (PCFF). Full details of this parameterisation can be found in ref. 17. All structural feature analysis was performed using Gaussian 09,²⁵ and full details of the model chemistries, calculation methods and spectra generation can be found in section S6.

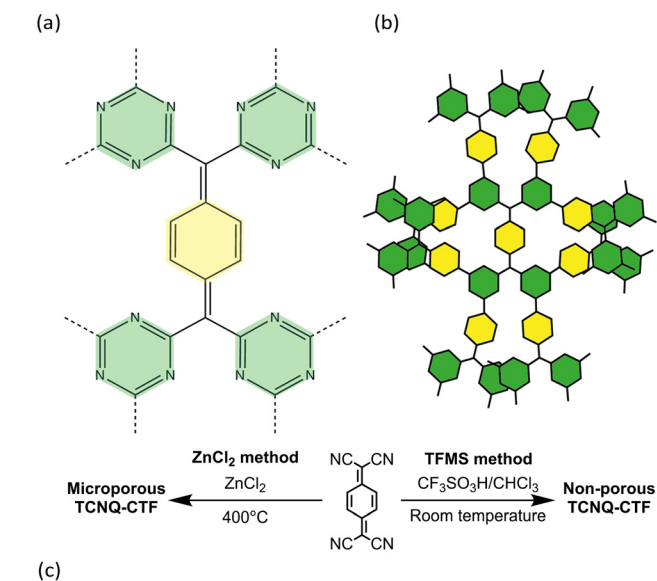


Fig. 1 (a) The chemical structure of the idealised TCNQ-CTF polymer structure with the generated triazine ring highlighted in green and the built-in *p*-quinodimethane moiety highlighted in yellow. (b) A section of the TCNQ-CTF framework highlighting the ease with which a disordered framework is formed through small deviations from ideal bond and dihedral angles. (c) The two approaches to synthesise TCNQ-CTF from the TCNQ monomer, (i) the ZnCl_2 method, that produces an amorphous but highly porous polymer, or (ii) the TFMS method that produces an amorphous non-porous polymer.



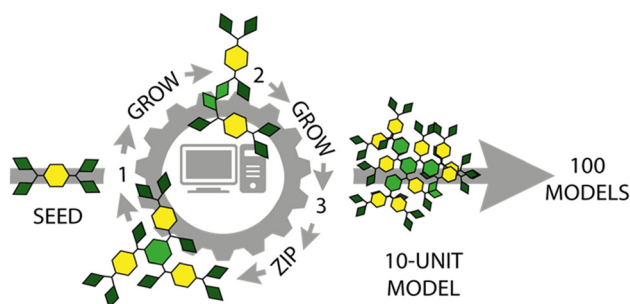


Fig. 2 The Ambuild model generation process. A TCNQ building block is seeded to give 1. Then a *growBlocks* step is undertaken whereby the cyano group (dark green) reacts to form an imine (light green) named intermediate 2. This process is repeated to give intermediate 3. At this point a *zipBlocks* test is undertaken and if successful a triazine ring is formed (light green hexagon). This process is repeated until there are 10 units within the model and this whole process is repeated a further 99 times to give a total of 100 independent models.

Results and discussion

In the previous ZnCl_2 -catalysed synthesis of TCNQ-CTF, an amorphous material was formed and triazine rings were the sole resulting structural feature.⁹ Our TFMS-catalysed synthesis also yields an amorphous product; however, the experimental spectra cannot be rationalised by considering triazine rings as the only structural feature present in the network.

Fig. 3 outlines the structural features identified *via* our computational synthesis approach and their prevalence across the 100 clusters produced. A full list of the structural features identified and their prevalence in the cluster models can be found in section S5. Amorphous networks are very challenging to analyse due to the limited characterisation techniques available. Some chemical functionality can be identified through IR spectroscopy or solid-state NMR, but it is often difficult to distinguish between similar groupings of chemical functionalities or structural features. Therefore, it is possible to miss functionality that may not be immediately obvious or is unexpected from the complete reaction taking place. This is a particular challenge in amorphous networks, where intermediates, otherwise not expected to be observed, may remain as they are fixed into their position within the polymer structure and so cannot react further, particularly in later stages of the network formation. Although *triazine* rings were one of the most common features present, with 19 counted across the clusters, the distribution was dominated by the closely related *triazocine* feature alongside macrocycles *triangle C* and *12-ring* (42, 39 and 25 observed, respectively). Previously identified in our P1 study,¹⁷ *4-ring* and *8-ring* features were also observed in our TCNQ-CTF clusters. This range of structural features contributes to the amorphicity of the material. We expect that this broader structural diversity compared to P1 arises because of the difference in structure and functionality of the monomer. The 1,4-dicyanobenzene monomer of P1 possesses two cyano groups *para* to one another, whereas the TCNQ monomer has

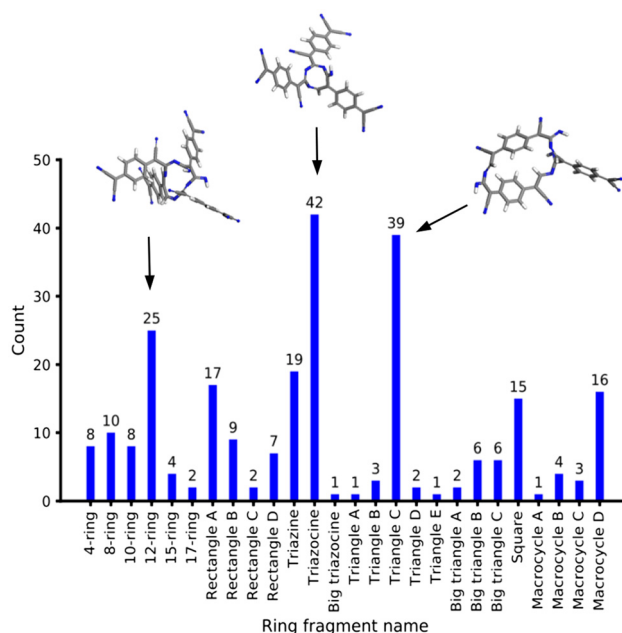


Fig. 3 Structural features found within the amorphous TCNQ-CTF formed *via* a TFMS catalysed synthesis. A full list of structural features and associated images is presented in Fig. S5. The insets show the most commonly observed features of a 12-ring, triazocine, and triangle C. In ZnCl_2 -catalysed synthesis of TCNQ-CTF, triazine rings were the sole feature identified.

four cyano groups, with two at each end separated by a single carbon atom. This reduction in distance, and variation in angle between cyano groups in the TCNQ monomer, leads to a wider range of bonding opportunities between the building blocks, introducing much greater diversity in macrocycle formation.

This contrasts with the structural composition of P1, where it was found that triazine rings were most prevalent as one would expect for this reaction pathway.¹⁷ Additionally, several 'pre-rings' were identified in the clusters, including *pre-4-rings*, *pre-triazines* and *pre-triazocines*. The *pre-4-ring* was the most prevalent feature overall, with 314 counted across the models. Notably, no *pre-8-rings* were observed, a feature identified in our P1 study.¹⁷

The experimental IR spectrum of TCNQ-CTF synthesised using a TFMS catalysed synthesis, shown in Fig. 4(a) in black, exhibits peaks at $\sim 1200\text{ cm}^{-1}$, $\sim 1500\text{ cm}^{-1}$, $\sim 2100\text{ cm}^{-1}$, $\sim 2200\text{ cm}^{-1}$, $\sim 2350\text{ cm}^{-1}$ and a broad peak with features at $\sim 3200\text{ cm}^{-1}$, $\sim 3350\text{ cm}^{-1}$, $\sim 3450\text{ cm}^{-1}$ and $\sim 3600\text{ cm}^{-1}$. The peaks at $\sim 2200\text{ cm}^{-1}$ and $\sim 2350\text{ cm}^{-1}$ can be attributed to unreacted cyano groups. We accounted for the presence of atmospheric CO_2 by calculating its IR spectrum (Fig. S46) and obtained a peak overlapping a cyano group peak at $\sim 2350\text{ cm}^{-1}$. Although the peaks at $\sim 1500\text{ cm}^{-1}$ and $\sim 1200\text{ cm}^{-1}$ have previously been assigned to triazine rings, and indeed our calculated spectra in this study support this, all ring and pre-ring calculated spectra possess peaks in these regions originating from the C=C and C=N bonds produced



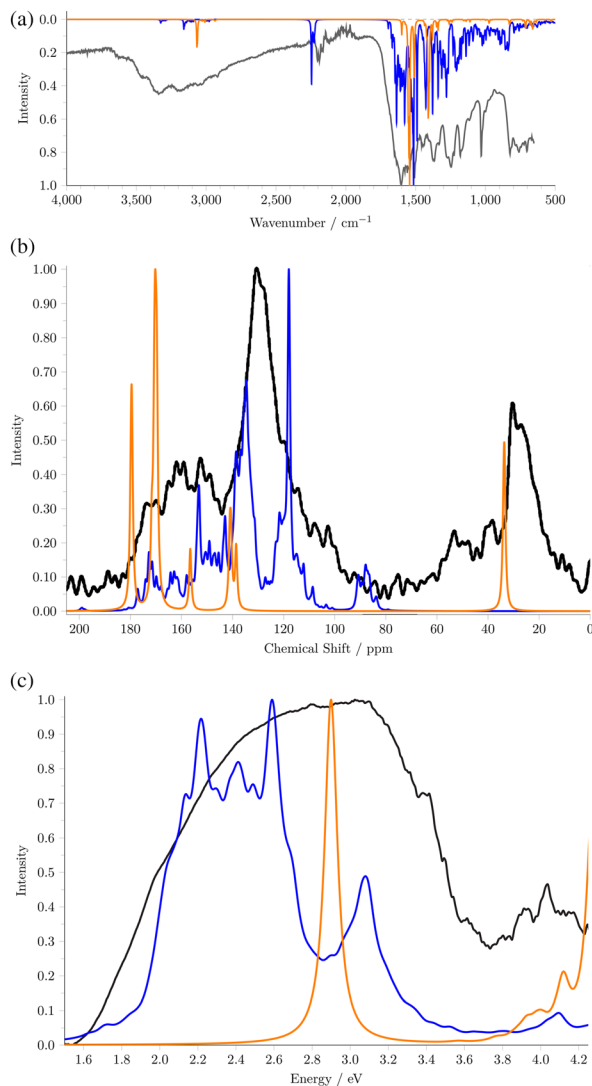


Fig. 4 The (a) IR, (b) NMR, and (c) UV-Vis spectra of our Ambuild-derived computed models (blue), weighted according to the statistics in Fig. 3, and reduced models (orange), compared to the experimental spectra of the synthesised TFMS acid catalysed TCNQ-CTF (black). See Fig. S52 for an expanded version of the IR spectrum.

upon macrocycle formation. This demonstrates the difficulty in rationalising a diverse, amorphous structure using only IR spectroscopy—the complexity of the spectrum cannot be rationalised by triazine rings alone. Upon analysis of the calculated spectra (Fig. S15–45(a)), the peak at $\sim 2100\text{ cm}^{-1}$ can be attributed to charged pre-ring intermediates present in the network, specifically stretches between the carbocation and neighbouring carbon and nitrogen atoms.¹⁷ The peaks at $\sim 3200\text{ cm}^{-1}$ and $\sim 3350\text{ cm}^{-1}$ arise from C–H stretches in the phenyl rings. It is well-known that porous materials readily adsorb water and carbon dioxide,¹⁷ and although TCNQ-CTF was found to be largely non-porous, these species are still able to adsorb onto the material's surface. We calculated the IR spectrum of a water molecule (Fig. S47(a)), giving a peak at

$\sim 3650\text{ cm}^{-1}$ which likely explains the experimental feature at $\sim 3600\text{ cm}^{-1}$.

Due to the presence of acid from the TFMS synthesis, it is reasonable to expect hydronium ions to form from water, and its calculated IR spectrum (Fig. S48(a)) exhibits a strong peak at $\sim 3450\text{ cm}^{-1}$ and further peaks at $\sim 3400\text{ cm}^{-1}$, $\sim 1600\text{ cm}^{-1}$ and $\sim 900\text{ cm}^{-1}$. Each of these peaks is observed in the experimental spectrum. The combined weighted IR spectrum (Fig. 4(a), blue) derived by statistically combining the individual spectra of 25 identified fragments (Fig. S16–40) is a good overall match to experiment. The additional peaks arising from carbon dioxide, water and the hydronium ion can be found in Fig. S46–48.

The weighted calculated NMR spectrum (Fig. 4(b), blue) is a good match to experiment (the full experimental spectrum is shown in Fig. S8) between 70–200 ppm, suggesting the structural features identified in our clusters dominate within the synthesised material.

As none of our calculated models show peaks at chemical shifts larger than 200 ppm, we choose to plot our calculated NMR spectra over the range of ~ 0 –200 ppm. The most intense peak of the calculated spectrum at 120 ppm can be attributed to unreacted cyano groups present in the material, which will naturally be overestimated in the fragment approach considered here. The peaks found between 90–125 ppm arise from the carbon atom adjacent to the cyano groups, becoming more deshielded when one of the cyano groups becomes an imine when participating in bonding within a macrocyclic ring.

Peaks from 150–165 ppm belong to phenyl group carbons, becoming more deshielded the closer to the cyano groups they are. In the calculated spectra, the only peak unique to one specific feature is that at around 200 ppm from the carbon atoms participating in the 4-ring. The experimentally observed feature at 230 ppm is suggested to be a spinning side band of the intense peak at 130 ppm, with an assigned matching band observed as part of the dominant peak at ~ 30 ppm.

The experimental UV-Vis spectrum (Fig. S6) has a broad high intensity peak from 1.5–3.5 eV and further lower-intensity peaks at 4.1 eV and 4.8 eV. This suggests the material has an optical gap of around 1.5 eV. The weighted calculated UV-Vis spectrum (Fig. 4(c), blue) shows a broad set of peaks between ~ 1.5 and 3.4 eV in-line with the experimental UV-Vis spectrum. The peaks at lower values between 1.5 and 2.2 eV appear strongly in the 4-, 8- and 10-ring fragments, whereas peaks between 2.2 and 2.8 eV are common throughout all fragments but are particularly dominant in triazocine fragments (Fig. S27 and S28) and triangles A (Fig. S29 and S34), and triangle E (Fig. S23). The peak at ~ 3.1 eV is particularly dominant in rectangles A and B (Fig. S22 and S23), and triangles C and D (Fig. S31 and S32). The small peak at ~ 4.1 eV is not prominent in any fragment but does feature in rectangle A (Fig. S22), triangle A (Fig. S29), and macrocycle B (Fig. S39).

We note that five of our identified fragments yield very low ($\ll 1$ eV) excitation energies, with calculations suggesting that these fragments may have triplet (*i.e.*, diradical) character. Given the small timescales of our Ambuild artificial synthesis



calculations compared to experiment, this “instability” may be representative of an incomplete artificial reaction. In the fully reacted system, we would therefore expect to see fewer pre-rings than we currently observe in the clusters. To avoid artificially biasing the resultant weighted spectra, we have only included contributions from the 25 identified “stable” fragments—the spectra in Fig. 4 do not include any contributions from these five “unstable” fragments.

We emphasise however that here, we are considering isolated fragments, which do not account for any of the longer-range structure or interactions of the real-world polymer, which may potentially stabilise such motifs.

We also note that we are considering around 40 fragments identified from a subset of 100 small clusters, so we may not have captured all possible structural environments. In addition to this, several of the studied fragments are similar in composition and functionality. It is incredibly challenging to assign specific activities to single sites with absolute certainty, as similar structures will give rise to similar characterisation spectra. We also acknowledge that as our material is amorphous, there may be different local structural environments and functionalities. This may increase the complexity in establishing structure–property relationships for target applications with our current knowledgebase.

Assessing the experimental and weighted calculated spectra as a whole, we can see that the set of peaks in the NMR at ~30 ppm and peaks between 2.6 and 3.0 eV and above ~3.8 eV in the UV–Vis spectra are not fully rationalised. In particular, whilst part of the peaks at ~30 ppm in the NMR can be attributed to the spinning side band for the intense peak at 130 ppm, the peak is too large to be solely due to that side band. Our models could not identify the remaining contributions to this peak. This suggests that either additional features are produced in the experimental synthesis that we are yet to identify, or that adsorbed species, such as residual solvent, are present.¹¹ To explore the possibility of as-yet unidentified structural features being the origin of these peaks, we consider the potential for alternative reactions. We note the peak is within the region we would expect aliphatic carbons to appear. It is known that TFMS is able to catalyse the hydrogenation of alkanes,²⁶ therefore we consider this possibility.

Two models were considered based on a fragment of the idealised CTF polymer shown in Fig. 1(a). In the first model, one of the two alkene bonds is reduced, and in the second model both alkene bonds are reduced. The NMR spectrum was then calculated for both fragments. Full details are given in section S7. We see that both models have a dominant peak at ~30 ppm (Fig. S50(b) and S51(b)), which when combined and compared to the experimental spectrum (Fig. 4(b), orange) are a good match to the previously unidentified set of peaks. Therefore, we assign these as due to the presence of aliphatic groups caused by the reduction (full or partial) of the 1,4-cyclohexadiene rings. The UV–Vis spectrum was also calculated for both fragments (Fig. S50(c) and S51(c)) which when combined is compared to the experimental spectrum in Fig. 4(c) – orange line. A good match is again observed, with a

peak at ~2.9 eV (originating from reduced model 1) and a peak starting at ~3.9 eV (originating from reduced model 2). For completeness, the IR spectrum was also calculated for both fragments, shown in Fig. S50(a) and S51(a), which were again combined and compared to the experimental spectrum in Fig. 4(a) – orange line. We can see that the combined spectrum is again consistent with the experimental spectrum.

Considering the experimental spectra and the calculated spectra together, they can only be rationalised through our approach of mimicking the synthetic method to identify the full range of structural features that can form.

Our approach highlights the breadth of structural features that form when a TFMS-acid catalysed approach is used to generate TCNQ-CTF. A number of these structural features identified are difficult to synthesise in isolation but have a wide range of potential uses, and so are exciting target chemistries for incorporation into polymer materials. For example, macrocyclic C=N groups can be classed as secondary ketimines, which are popular in coordination chemistry as salen ligands and Schiff bases.^{27–31} Additionally, the larger macrocyclic rings have the potential for applications available to polyimines, such as their use as CANs to achieve thermoset-like properties, recycling and self-healing.^{20–22} Thermoset-like properties, which are obtained from the highly crosslinked polymer backbone, help to increase rigidity and mechanical strength within the materials.²² Due to the strong covalent bonds present, framework rigidity is maintained even at high temperatures, giving various engineering applications. Self-healing and recycling properties are also advantageous when considering the global requirement to reduce the quantity of waste generated, which is beneficial from both an environmental and economic viewpoint. Self-healing polymers, which utilise the framework structure to ‘heal’ the effects of degradation over time, have been used in biomedicine, electronics and coatings, extending the lifetime of the material.³² The free primary ketimines produced when the cyano carbon bonds to another nitrogen atom provides the possibility for post-functionalisation, further broadening the range of potential applications of this diverse material.

Conclusions

We have demonstrated a new way to synthesise amorphous TCNQ-CTF with additional structural diversity compared to the previously reported ZnCl₂ method. This approach uses a room temperature synthesis with TFMS acid-catalysed cycloaddition.

Alongside the experimental synthesis, ‘artificial synthesis’, growing a series of 100 cluster models of TCNQ-CTF, is used to probe potential structural features generated in this kinetically controlled reaction. To help interpret the resultant clusters, we have developed an efficient categorisation protocol, allowing the prevalence of different structural features to be automatically identified. Using these statistical data and a series of structural fragments derived from the clusters, we have



efficiently rationalised the experimentally observed IR, NMR, and UV-Vis spectra of the resultant material. Importantly, the spectra can only be rationalised assuming a diverse set of structural features form experimentally, highlighting the importance of allowing for deviation from the thermodynamic product when modelling these exciting materials.

The structural diversity in the synthesised TCNQ-CTF thus provides additional chemical functionality, leading to possible applications across a broad range of areas, including within coordination chemistry, and as covalent adaptable networks.

Author contributions

Catherine Mollart and Ellena Sherrett: conceptualisation, methodology, data collection, analysis and manuscript preparation. Patrick Heasman: conceptualisation and synthesis. Michael J. G. Peach: data analysis. Adam Rowling, Lewis Beck, Ellie Varley, and David Seed: data collection and analysis. Abbie Trewin: conceptualisation, editing, and supervision.

Conflicts of interest

There are no conflicts to declare.

Data availability

The data supporting this article have been included as part of the supplementary information (SI). Supplementary information: synthetic details, computational methodology details, fragment models. See DOI: <https://doi.org/10.1039/d5py00872g>.

The code for Ambuild can be found at <https://github.com/linucks/ambuild>.

Acknowledgements

The authors would like to thank the High End Computing facility at Lancaster University, which was used to run all the Ambuild simulations and Gaussian calculations discussed here.

References

- 1 X. Wang, T. Han, J. Gong, P. Alam, H. Zhang, J. W. Y. Lam and B. Z. Tang, Diversity-Oriented Synthesis of Functional Polymers with Multisubstituted Small Heterocycles by Facile Stereoselective Multicomponent Polymerizations, *Macromolecules*, 2022, **55**(11), 4389–4401, DOI: [10.1021/acs.macromol.2c00319](https://doi.org/10.1021/acs.macromol.2c00319).
- 2 X. Zhu, C. Tian, S. M. Mahurin, S.-H. Chai, C. Wang, S. Brown, G. M. Veith, H. Luo, H. Liu and S. Dai, A Superacid-Catalyzed Synthesis of Porous Membranes Based on Triazine Frameworks for CO₂ Separation, *J. Am. Chem. Soc.*, 2012, **134**(25), 10478–10484, DOI: [10.1021/ja304879c](https://doi.org/10.1021/ja304879c).
- 3 S. Hug, L. Stegbauer, H. Oh, M. Hirscher and B. V. Lotsch, Nitrogen-Rich Covalent Triazine Frameworks as High-Performance Platforms for Selective Carbon Capture and Storage, *Chem. Mater.*, 2015, **27**(23), 8001–8010, DOI: [10.1021/acs.chemmater.5b03330](https://doi.org/10.1021/acs.chemmater.5b03330).
- 4 S. N. Talapaneni, T. H. Hwang, S. H. Je, O. Buyukcakil, J. W. Choi and A. Coskun, Elemental-Sulfur-Mediated Facile Synthesis of a Covalent Triazine Framework for High-Performance Lithium-Sulfur Batteries, *Angew. Chem., Int. Ed.*, 2016, **55**(9), 3106–3111, DOI: [10.1002/anie.201511553](https://doi.org/10.1002/anie.201511553).
- 5 J. Xie, S. A. Shevlin, Q. Ruan, S. J. A. Moniz, Y. Liu, X. Liu, Y. Li, C. C. Lau, Z. X. Guo and J. Tang, Efficient visible light-driven water oxidation and proton reduction by an ordered covalent triazine-based framework, *Energy Environ. Sci.*, 2018, **11**(6), 1617–1624, DOI: [10.1039/C7EE02981K](https://doi.org/10.1039/C7EE02981K).
- 6 R. Palkovits, M. Antonietti, P. Kuhn, A. Thomas and F. Schüth, Solid Catalysts for the Selective Low-Temperature Oxidation of Methane to Methanol, *Angew. Chem., Int. Ed.*, 2009, **48**(37), 6909–6912, DOI: [10.1002/anie.200902009](https://doi.org/10.1002/anie.200902009).
- 7 S. Vijayakrishnan, J. W. Ward and A. I. Cooper, Discovery of a Covalent Triazine Framework Photocatalyst for Visible-Light-Driven Chemical Synthesis using High-Throughput Screening, *ACS Catal.*, 2022, **12**(16), 10057–10064, DOI: [10.1021/acscatal.2c02743](https://doi.org/10.1021/acscatal.2c02743).
- 8 M. Dinari, N. Mokhtari, S. Taymouri, M. Arshadi and A. Abbaspourrad, Covalent polybenzimidazole-based triazine frameworks: A robust carrier for non-steroidal anti-inflammatory drugs, *Mater. Sci. Eng., C*, 2020, **108**, 110482, DOI: [10.1016/j.msec.2019.110482](https://doi.org/10.1016/j.msec.2019.110482).
- 9 H. Tran, R. Gurnani, C. Kim, G. Pilania, H.-K. Kwon, R. P. Lively and R. Ramprasad, Design of functional and sustainable polymers assisted by artificial intelligence, *Nat. Rev. Mater.*, 2024, **9**(12), 866–886, DOI: [10.1038/s41578-024-00708-8](https://doi.org/10.1038/s41578-024-00708-8).
- 10 L. Gao, J. Lin, L. Wang and L. Du, Machine Learning-Assisted Design of Advanced Polymeric Materials, *Acc. Mater. Res.*, 2024, **5**(5), 571–584, DOI: [10.1021/accountsmr.3c00288](https://doi.org/10.1021/accountsmr.3c00288).
- 11 S. Ren, M. J. Bojdys, R. Dawson, A. Laybourn, Y. Z. Khimyak, D. J. Adams and A. I. Cooper, Porous, Fluorescent, Covalent Triazine-Based Frameworks Via Room-Temperature and Microwave-Assisted Synthesis, *Adv. Mater.*, 2012, **24**, 2357–2361, DOI: [10.1002/adma.201200751](https://doi.org/10.1002/adma.201200751) (accessed 2023/09/04).
- 12 H. Wang, D. Jiang, D. Huang, G. Zeng, P. Xu, C. Lai, M. Chen, M. Cheng, C. Zhang and Z. Wang, Covalent triazine frameworks for carbon dioxide capture, *J. Mater. Chem. A*, 2019, **7**(40), 22848–22870, DOI: [10.1039/C9TA06847C](https://doi.org/10.1039/C9TA06847C).
- 13 A. Rengaraj, P. Puthiaraj, Y. Haldorai, N. S. Heo, S.-K. Hwang, Y.-K. Han, S. Kwon, W.-S. Ahn and Y. S. Huh, Porous Covalent Triazine Polymer as a Potential Nanocargo for Cancer Therapy and Imaging, *ACS Appl. Mater.*



- Interfaces*, 2016, **8**(14), 8947–8955, DOI: [10.1021/acsami.6b00284](https://doi.org/10.1021/acsami.6b00284).
- 14 R. Palkovits, M. Antonietti, P. Kuhn, A. Thomas and F. Schüth, Solid Catalysts for the Selective Low-Temperature Oxidation of Methane to Methanol, *Angew. Chem., Int. Ed.*, 2009, **48**(37), 6909–6912, DOI: [10.1002/anie.200902009](https://doi.org/10.1002/anie.200902009) (accessed 2023/09/15).
 - 15 W. Huang, Q. He, Y. Hu and Y. Li, Molecular Heterostructures of Covalent Triazine Frameworks for Enhanced Photocatalytic Hydrogen Production, *Angew. Chem., Int. Ed.*, 2019, **58**(26), 8676–8680, DOI: [10.1002/anie.201900046](https://doi.org/10.1002/anie.201900046) (accessed 2023/09/15).
 - 16 P. Kuhn, M. Antonietti and A. Thomas, Porous, Covalent Triazine-Based Frameworks Prepared by Ionothermal Synthesis, *Angew. Chem., Int. Ed.*, 2008, **47**, 3450–3453, DOI: [10.1002/anie.200705710](https://doi.org/10.1002/anie.200705710) (accessed 2023/09/04).
 - 17 C. Mollart, S. Holcroft, M. J. G. Peach, A. Rowling and A. Trewin, Artificial synthesis of covalent triazine frameworks for local structure and property determination, *Phys. Chem. Chem. Phys.*, 2022, **24**(34), 20025–20029, DOI: [10.1039/D2CP02430F](https://doi.org/10.1039/D2CP02430F).
 - 18 Y. Li, S. Zheng, X. Liu, P. Li, L. Sun, R. Yang, S. Wang, Z.-S. Wu, X. Bao and W.-Q. Deng, Conductive Microporous Covalent Triazine-Based Framework for High-Performance Electrochemical Capacitive Energy Storage, *Angew. Chem., Int. Ed.*, 2018, **57**(27), 7992–7996, DOI: [10.1002/anie.201711169](https://doi.org/10.1002/anie.201711169) (accessed 2023/09/14).
 - 19 C. Mollart, P. Heasman, E. Sherrett, P. A. T. J. Fletcher, P. Fayon, J. M. H. Thomas, V. Franckevičius, M. J. G. Peach and A. Trewin, A New Combined Computational and Experimental Approach to Characterize Photoactive Conjugated 3D Polymers, *Small*, 2025, **21**(9), 2407187, DOI: [10.1002/smll.202407187](https://doi.org/10.1002/smll.202407187).
 - 20 T. Han, H. Deng, Z. Qiu, Z. Zhao, H. Zhang, H. Zou, N. L. C. Leung, G. Shan, M. R. J. Elsegood, J. W. Y. Lam, *et al.*, Facile Multicomponent Polymerizations toward Unconventional Luminescent Polymers with Readily Openable Small Heterocycles, *J. Am. Chem. Soc.*, 2018, **140**(16), 5588–5598, DOI: [10.1021/jacs.8b01991](https://doi.org/10.1021/jacs.8b01991).
 - 21 B. H. Rotstein, S. Zaretsky, V. Rai and A. K. Yudin, Small Heterocycles in Multicomponent Reactions, *Chem. Rev.*, 2014, **114**(16), 8323–8359, DOI: [10.1021/cr400615v](https://doi.org/10.1021/cr400615v).
 - 22 P. Yu, H. Wang, T. Li, G. Wang, Z. Jia, X. Dong, Y. Xu, Q. Ma, D. Zhang, H. Ding, *et al.*, Mechanically Robust, Recyclable, and Self-Healing Polyimine Networks, *Adv. Sci.*, 2023, **10**(19), 2300958, DOI: [10.1002/advs.202300958](https://doi.org/10.1002/advs.202300958) (accessed 2024/08/06).
 - 23 C. J. Kloxin, T. F. Scott, B. J. Adzima and C. N. Bowman, Covalent Adaptable Networks (CANs): A Unique Paradigm in Cross-Linked Polymers, *Macromolecules*, 2010, **43**(6), 2643–2653, DOI: [10.1021/ma902596s](https://doi.org/10.1021/ma902596s).
 - 24 U. Nations, *Sustainable Development*, 2025. <https://sdgs.un.org/goals/goal12> (accessed 2025).
 - 25 M. J. Frisch, G. W. Trucks, H. B. Schlegel, G. E. Scuseria, M. A. Robb, J. R. Cheeseman, G. Scalmani, V. Barone, B. Mennucci, G. A. Petersson, *et al.*, *Gaussian 09 Revision E.01*, 2015.
 - 26 K. Shimizu, H. Karamatsu, A. Inaba, A. Suganuma and I. Saito, Solubilization of Taiheiyo coal under mild conditions without gaseous hydrogen: catalysis by trifluoromethanesulfonic acid, *Fuel*, 1995, **74**(6), 853–859, DOI: [10.1016/0016-2361\(95\)00010-3](https://doi.org/10.1016/0016-2361(95)00010-3).
 - 27 P. G. Cozzi, Metal–Salen Schiff base complexes in catalysis: practical aspects, *Chem. Soc. Rev.*, 2004, **33**(7), 410–421, DOI: [10.1039/B307853C](https://doi.org/10.1039/B307853C).
 - 28 E. C. Constable and C. E. Housecroft, 8.01 – Ligand and Metalloligand Design for Macrocycles, Multimetallic Arrays, Coordination Polymers, and Assemblies, in *Comprehensive Inorganic Chemistry II*, ed. J. Reedijk and K. Poepelmeier, Elsevier, 2nd edn, 2013, pp. 1–29.
 - 29 A. G. De Candia, J. P. Marcolongo and L. D. Slep, A new ruthenium nitrosyl species based on a pendant-arm 1,4,8,11-tetraazacyclotetradecane (cyclam) derivative: An experimental and theoretical study, *Polyhedron*, 2007, **26**(16), 4719–4730, DOI: [10.1016/j.poly.2007.04.038](https://doi.org/10.1016/j.poly.2007.04.038).
 - 30 K. Krämer, M. Schmitz, H. Kelm, C. van Wüllen and H.-J. Krüger, Unexpected Reduction of a Coordinated Diazapyridinophane Ligand Bound to Chromium(III) Ion Leading to Delocalization of the Unpaired Electron across Two Isolated Pyridine Units, *Chem. – Eur. J.*, 2024, **30**(5), e202301099, DOI: [10.1002/chem.202301099](https://doi.org/10.1002/chem.202301099) (accessed 2024/08/06).
 - 31 S. K. Schoustra and M. M. J. Smulders, Metal Coordination in Polyimine Covalent Adaptable Networks for Tunable Material Properties and Enhanced Creep Resistance, *Macromol. Rapid Commun.*, 2023, **44**(5), 2200790, DOI: [10.1002/marc.202200790](https://doi.org/10.1002/marc.202200790) (accessed 2024/08/06).
 - 32 S. Wang and M. W. Urban, Self-healing polymers, *Nat. Rev. Mater.*, 2020, **5**(8), 562–583, DOI: [10.1038/s41578-020-0202-4](https://doi.org/10.1038/s41578-020-0202-4).

